



Role of ocean–atmosphere interactions on contrasting characteristics of two cyclones over the Arabian Sea

P. Ipsita¹ · V. Rakesh¹ · G. N. Mohapatra¹

Received: 28 February 2023 / Accepted: 14 August 2023 / Published online: 31 August 2023
© The Author(s), under exclusive licence to Springer-Verlag GmbH Austria, part of Springer Nature 2023

Abstract

The role of ocean–atmosphere interaction in modulating the track and intensity of two cyclonic storms, Nisarga and Nanauk, which originated from almost similar locations in June in the Arabian Sea with completely different tracks, is investigated in this study. Sea surface temperature (SST), steering flow, relative vorticity, latent heat flux (LHF), specific humidity, vertical wind shear (VWS), outgoing longwave radiation (OLR), convective available potential energy (CAPE), and Madden–Julian oscillation (MJO) phases are analyzed to elucidate the causes of contrasting characteristics of these two cyclones. During the progression and intensification of the storm Nanauk, SST decreased drastically (magnitude of ~ 4 °C), while VWS anomaly is found to be increased (~ 8 ms⁻¹), followed by entrainment of dry air leading to a decrease in upward LHF anomaly (~ 3.5 to 4 J m⁻²) hindering further moisture supply. Moreover, just before the storm initiation, the CAPE anomaly was around -800 to -1000 J kg⁻¹ and the MJO condition was also unfavorable for the continuous intensification of the cyclone. All these factors contributed to the quick dissipation of cyclone Nanauk. However, high SST (~ 31 °C) along with other favorable atmospheric conditions contrary to cyclone Nanauk provided a conducive environment for Nisarga to intensify and prevail. A high-pressure anticyclonic circulation at the eastern side of Nisarga over Indian land dragged the storm north-eastwards across the Maharashtra coast. The convective phase of MJO (magnitude > 1) along with the strong lower tropospheric westerly wind at the west side of the convective system also helped cyclone Nisarga to propagate eastward.

1 Introduction

Tropical cyclones (TCs) are associated with strong wind, storm surges, and flooding, that give rise to significant damage to property and infrastructure along with a large number of casualties (Charney and Eliassen 1964; Rappaport 2000; Webster 2008). Globally, the intensity of TCs has increased in the last decades (Collins et al. 2019; Kossin et al. 2020) by around 5% per decade since 1979. Though the bi-modal frequency (McBride 1995) of North Indian Ocean cyclones contributes only 6% of the total global tropical cyclones (Singh et al. 2020a), the socio-economic impact of a cyclone is considerably huge in India, due to the dense population along the coastal regions (Beal et al. 2020; Deo 2011; Dube et al. 2009; Needham 2015). Though, relatively cold

waters in the Arabian Sea contribute only 2% of the annual global frequency of cyclones (Knapp et al. 2010), in the present scenario, rapid warming of the Arabian Sea (Roxy et al. 2019) can result in the formation of more frequent and intense TCs (Mohapatra et al. 2015; Murakami et al. 2017; Sobel et al. 2016) that can cause severe damage to life and property. Hence, understanding the characteristics and identifying factors modulating such cyclones is crucial for advanced prediction of such cyclones using dynamical models. Despite recent improvements in the forecasting of such natural disasters, rapid intensification and unusual tracks of tropical cyclones make forecasting a challenging affair adding risks to coastal communities (Emanuel 2017). Generally, model performance is comparatively better in track prediction than intensity prediction, which is still challenging for modeling communities (DeMaria et al. 2014; Mohapatra et al. 2013a, b, 2017, 2018).

Heat transfer from the surface of the ocean through evaporative cooling by winds act as the major driving force while tropical cyclone passes through the ocean. In addition, atmospheric dynamical and thermodynamical properties play an important role in the genesis,

Responsible Editor: Clemens Simmer, Ph.D.

✉ P. Ipsita
ipsita.putatunda@gmail.com

¹ Earth and Engineering Sciences Division, CSIR Fourth Paradigm Institute, Bangalore 560037, India

intensification, and propagation of the tropical cyclone. Usually, in the summer monsoon season in India, vertical wind shear increases, which suppresses cyclone formation in the north Indian Ocean (Li et al. 2013; Xing and Huang 2013; Yanase et al. 2012). The intensity and track of the tropical cyclone are mainly controlled by dynamical forcing, environmental conditions, and their interactions with the ocean (Wang and Wu 2004).

Dry mid-troposphere (Emanuel et al. 2004) or vortex tilting (DeMaria 1996) can suppress TC intensification by decreasing convective buoyancy. Many studies on tropical cyclogenesis were conducted to understand the mechanism by which the cumulus convection organizes to develop a large-scale cyclonic vortex (Braun et al. 2013; Komaromi 2013; Zawislak 2013). Low-level vortex intensification increases convective activity in tropical mesoscale systems (Zehr 1992) and the convective updrafts and mesoscale vortices together can form strong cyclonic vorticity (Enagonio and Montgomery 2001). Cyclone generally draws energy from the ocean (Emanuel 1986), hence increasing enthalpy flux in the air–sea interface can increase TCs intensification (Emanuel 1999). Higher SST can increase the duration and intensity of cyclones (Emanuel 2000; Klotzbach 2006; Singh et al. 2020b; Wing et al. 2007). Studies showed that mean track and intensity estimation errors can be reduced with the incorporation of SST in the forecast model (Bongirwar et al. 2011; Mohanty et al. 2019). Previous studies have suggested that the track of tropical cyclones is a function of the deep-layer wind field, i.e., steering flow, (George and Gray 1976; Neumann 1992). The active phase of an eastward-propagating band of intra-seasonal variations (Madden and Julian 1971) called Madden–Julian Oscillation (MJO) also significantly affects the genesis as well as the intensification of tropical cyclones (Klotzbach 2014; Krishnamohan et al. 2012; Maloney and Hartmann 2001).

The above discussion shows that large-scale environmental flow plays a crucial role in the modulation of cyclonic storms. Understanding the role of ocean–atmosphere interaction and ocean subsurface conditions in regulating the track and intensity of the tropical cyclone is important to understand how these processes are represented in models which in turn is crucial for further improvement in such models. To be specific, the objective of this study is to investigate the role of ocean–atmosphere interaction in contrasting characteristics of two tropical cyclones, that originated in almost the same location over the Arabian Sea during the month of June. To meet this objective, we have selected two cyclones formed in the Arabian Sea such as Nisarga and Nanauk which had contrasting natures in terms of intensity and track. The remaining portion of the study is structured as follows. An overview of two tropical cyclones selected for the study is presented in Sect. 2. Section 3 gives data used

in the study and the methodology adopted. Major results are discussed in Sect. 4 followed by our conclusions.

2 Overview of cyclones Nisarga and Nanauk

A depression occurred on 1 June 2020 over the Arabian Sea basin just before the onset of the Indian summer monsoon and gradually intensified into severe cyclone Nisarga. Cyclone Nisarga is the most severe tropical cyclone since 1891 that strike the Maharashtra coast in the month of June, which makes Nisarga a special case to comprehend its characteristics. The complete track of the tropical cyclone Nisarga from the India Meteorological Department (IMD) is shown in Fig. 1a. A well-marked low pressure developed as a depression over the southeast Arabian Sea area on 31 May 2020 at 00 UTC on 1 June 2020 near 13.0° N and 71.4° E (<http://www.rsmcnewdelhi.imd.gov.in>). This depression further intensified into a deep depression during the next 24 h and further intensified as a cyclonic storm in another 12 h with a surface wind speed of 65 kmph. Cyclonic storm Nisarga then moved northward till 2 June 2020 morning. On 3 June 2020 at 00 UTC Nisarga intensified as a severe cyclonic storm with a wind speed of 92.6 kmph, and moved north-eastwards while crossing the Maharashtra coast close to the south of Alibag near 18.35° N and 72.95° E with a maximum wind speed of 111.12 kmph during 07 UTC to 09 UTC on 3 June 2020. Severe cyclonic storm Nisarga with a wind speed of 101 kmph weakened into cyclonic storm (74 kmph) and centered at 12 UTC on 3 June 2020, over interior Maharashtra, near 19.0° N and 73.7° E, 90 km east of Mumbai and 50 km north-north-west of Pune. The cyclonic storm then further weekend to a deep depression at 15 UTC on 3 June 2020 and then as a depression at 00 UTC on 4 June 2020, near 20.5° N and 76.0° E, over western parts of Vidarbha with 37 kmph surface wind speed. Figure 1c shows the surface wind speed (kmph) of cyclone Nisarga from 2 to 4 June 2020. A gradual decrease in surface pressure anomaly is associated with storm intensification (Fig. 2a–f). Starting on 30 May 2020, the surface pressure at the storm center started decreasing to a minimum on 3 June 2020. A well-marked anticyclonic high-pressure area was visible in the eastern India region. As the storm entered the land, the pressure increases and merged with the well-defined high-pressure area in the eastern part of peninsular India. A low-intensity precipitation (Fig. S1a) is observed in the pre-cyclonic period of Nisarga over the southeastern coast of the Arabian Sea. During the formation stage of TCs, precipitation, which is one of the major outcomes of convection associated with tropical cyclones (Groisman et al. 2004; Shephard et al. 2007), occurs generally due to low-intensity convection. As the storm intensified (Fig. S1b) and propagated north-eastward, the precipitation intensity

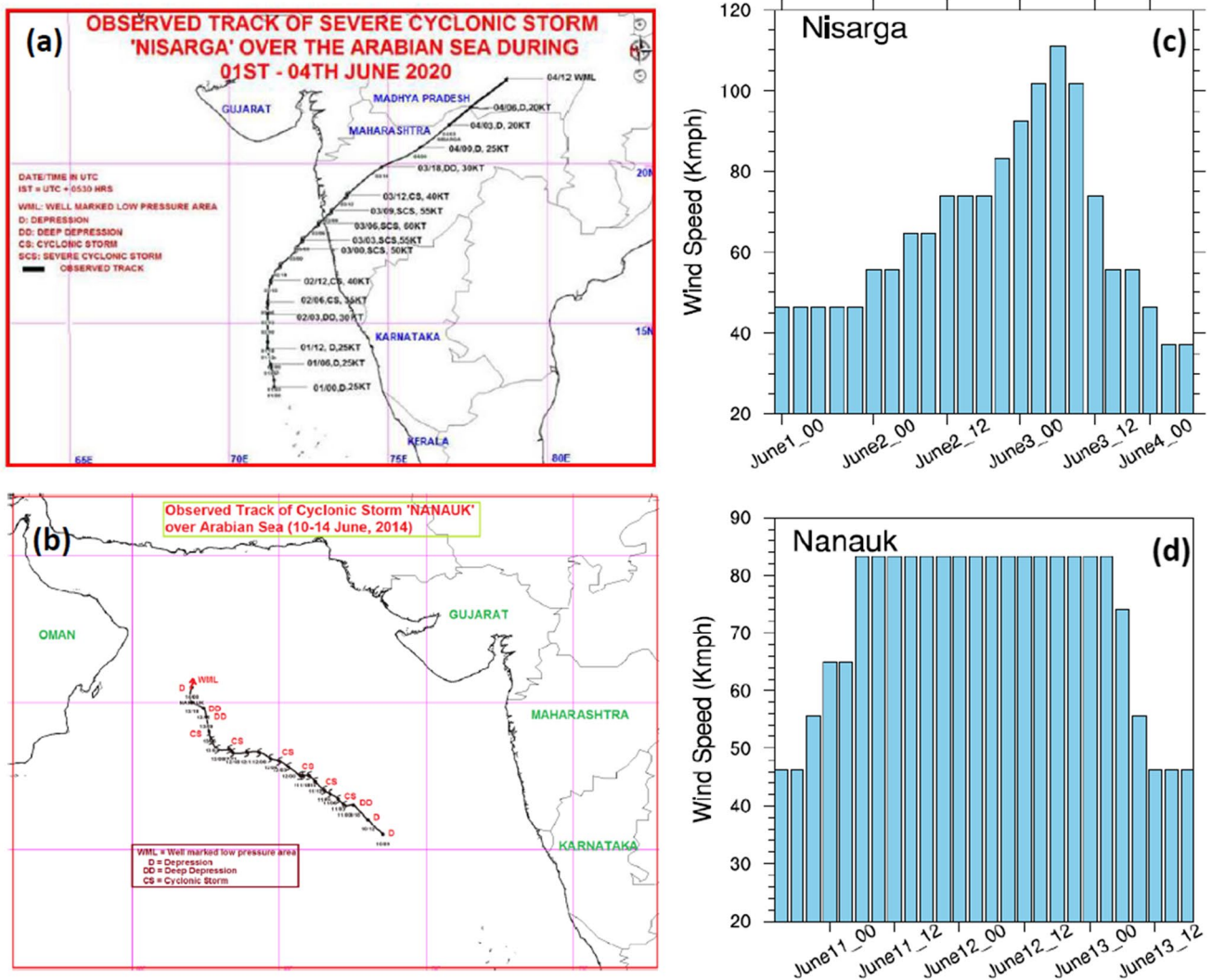


Fig. 1 Observed track from IMD for the cyclone Nisarga (a; Source: https://rsmcnewdelhi.imd.gov.in/uploads/report/26/26_f84c76_nisar_ga.pdf) and cyclone Nanauk (b; source: https://rsmcnewdelhi.imd.gov.in/uploads/report/26/26_c4b664_NANAUK.pdf); (c) change in surface wind speed (kmph) of cyclone Nisarga from 1 to 4 June 2020 and (d) cyclone Nanauk from 10 to 13 June 2014

increased and moved northward along the coast, following the track of the storm. A band of heavy rainfall surrounding the storm center known as the eyewall was also clearly visible (Fig. S1b). After passing the storm, the total surface precipitation anomaly was negative (Fig. S1c) spreading over a large part of the eastern Arabian sea. Various environmental factors (Rogers et al. 2003) can affect the precipitation structure and the precipitation structures associated with TCs are very complex and it varies from one case to another (Burpee and Black 1989).

Another cyclone event selected was cyclonic storm Nanauk which also originated from a similar region in the Arabian Sea like cyclone Nisarga, on 10 June 2014, and moved north-westwards in the Arabian Sea and depleted (Fig. 1b). In the case of cyclone Nanauk, a low-pressure

area formed on 9 June morning, 2014 over the east-central Arabian Sea, and with the impact of the active southwest monsoon surge (Fig. 2g–l), it intensified into depression in the afternoon of 10 June 2014 with a wind speed of 55.5 kmph (Fig. 1d). While progressing north-west wards, the depression intensified and became a cyclonic storm (CS) with an increased wind speed of ~65 kmph to ~83 kmph in the early morning of 11 June 2014. The storm was sustained as a cyclonic storm with a prevailing wind speed of ~83 kmph till 13 June morning. The CS over the west-central Arabian Sea weakened in the afternoon of 13 June 2014 into a deep depression (~55.5 kmph), and into a depression thereafter in the evening (~46 kmph) (Fig. 1d). The depression then weakened into a well-marked low-pressure area the next day morning over the same region.

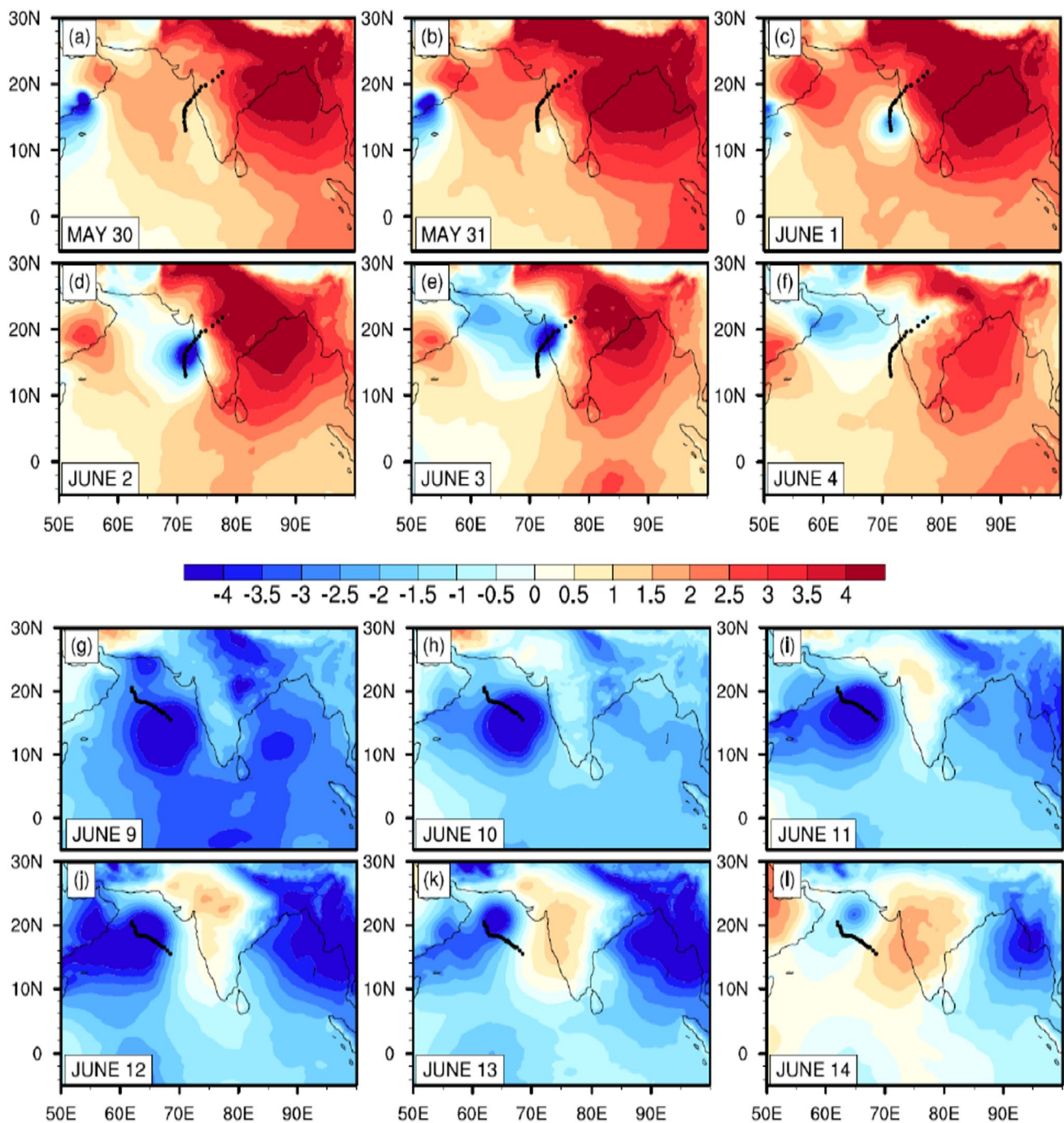


Fig. 2 Surface pressure anomaly (hPa); for cyclone Nisarga from 30 May to 4 June 2020 (a–f) and for cyclone Nanauk from 9 to 14 June 2014 (g–l)

Though some scattered rainfall is observed in the case of Nanauk, at the nearby area in the pre-cyclonic period (Fig. S1d), the precipitation intensity increased as the storm intensifies into a cyclone (Fig. S1e). After the passage of the storm, a negative precipitation anomaly is observed throughout the eastern Arabian Sea.

3 Data and methodology

This study used cyclone track and surface wind information, obtained from India Meteorological Department (IMD) Regional Specialised Meteorological Centre (RSMC) best track data. Daily SST data are obtained

from the Optimum Interpolation Sea Surface Temperature (OISST) data set, with 0.25° spatial resolution (Reynolds et al. 2007). Surface pressure, relative vorticity at 850 hPa, total surface precipitation, specific humidity averaged over 850 hPa to 550 hPa, Convective Available Potential Energy (CAPE), Outgoing Longwave Radiation (OLR) data, and zonal and meridional wind data are obtained from the ERA5, fifth-generation ECMWF reanalysis dataset. ERA5 data with 0.25° spatial resolution (Dee et al. 2011) are used in the present study. The vertical wind shear which is the difference between wind vectors at two different levels is calculated by taking the vector difference between 250 and 850 hPa. Environmental steering flow is calculated by taking the wind vector average of the layer from 850 to 300 hPa. Daily anomalies are calculated for all atmospheric parameters and SST with respect to the daily climatology. Anomalies of each parameter are calculated by taking daily data for the period 1979–2020 and 1979–2014 for Nisarga and Nanauk, respectively. This daily data have been averaged at each grid point for the entire period and then the difference between the actual data and the long-term mean for a particular day gives the daily anomaly. To enhance the understanding of the variability of each atmospheric and oceanic parameter, analysis has been performed for 7 days prior (25–31 May 2020 for Nisarga and 3–9 June 2014 for Nanauk), post (4–10 June 2020 for Nisarga and 14–20 June 2014 for Nanauk) and during (1–4 June 2020 for Nisarga and 10–14 June 2014 for Nanauk) the cyclone named as pre-cyclonic, post-cyclonic and cyclonic period, respectively, in rest of the discussion. Real-time multivariate MJO (RMM) index data are collected from the Australian Bureau of Meteorology in this study. RMM index data are used to understand the phase and amplitude of MJO as it plays an important role in the genesis and progression of the cyclone. The eight phases of RMM indicate different regions where active and suppressed convection associated with the MJO occurs. The major advantage of the RMM index is its real-time operational use as it does not need any time filtering. Wheeler and Hendon (2004) derived the RMM index to track the dynamical and convective signal of the MJO. RMM is obtained from the first two empirical orthogonal functions (EOFs) components (RMM1, RMM2) derived from the daily OLR anomalies and zonal winds at 850 hPa and 200 hPa averaged over 15° S to 15° N (Wheeler and Hendon 2004). RMM index moves anti-clockwise and when the MJO moves from west to east outside (inside) the center circle of the phase diagram, it is considered as strong (weak).

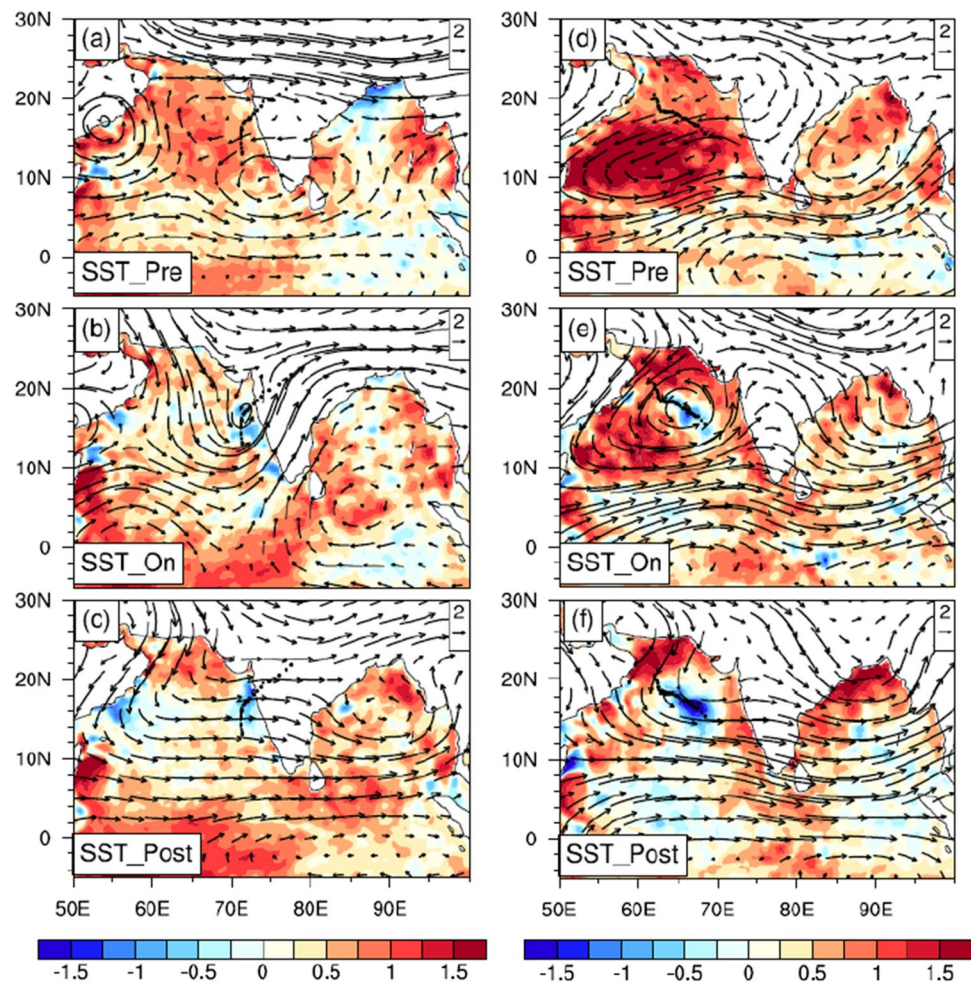
4 Results

There are several atmospheric and oceanic conditions that directly or indirectly control the genesis, intensification, and track of tropical cyclones (Chen et al. 2015; Gray 1979; Wang et al. 2004). The role of SST, environmental steering, relative vorticity, surface latent heat flux, specific humidity, relative vorticity, vertical wind shear, OLR, and CAPE along with MJO in the genesis, propagation, and intensification of two contrasting tropical cyclones over the Arabian Sea has been analyzed and results are presented below.

4.1 Sea surface temperature and environmental steering

SST anomaly is shown (Fig. 3) for the pre, post, and during the cyclonic period for both storms. High SST anomaly, about 1.2 – 1.4°C around the genesis center over the north-eastern part of the Arabian Sea is observed in the pre-cyclonic period for Nisarga (Fig. 3a) and Nanauk (Fig. 3d). This high value of SST provides a favorable environment and acts as the primary energy source for cyclogenesis and helps in the storm intensification (Chowdhury et al. 2020; Roxy et al. 2015, 2019; Sanap et al. 2020; Singh et al. 2020b). An earlier study (Sebastian and Behera 2015) over the Arabian Sea showed a high correlation (~ 0.73) between SST and the power dissipation index, the latter is an aggregate of storm intensity, frequency, duration, and provides a measure of total storm power (Emanuel 2005, 2007) and is proportional to the intensity of the cyclonic storm. In the pre-cyclonic period, both the storms show high SST anomaly (Fig. 3a, d) over the Arabian Sea. Comparatively higher anomaly is seen for the case of Nanauk, which can be due to various plausible reasons. Strong monsoonal winds force intense coastal and open-ocean upwelling in the Arabian Sea, and modulate evaporation and moisture transport towards India (Izumo et al. 2008), leaving a comparatively low SST near the west coast of the Arabian Sea. Further, El Niño-Southern Oscillation (ENSO) and Indian Ocean Dipole (IOD) events play a crucial role in modulating the temperature over the western Indian Ocean (Chowdary and Gnanaseelan 2007). Correlation between the eastern Pacific and global summer mean SST anomalies depicts a significant (99%) positive correlation ($r=0.6$) over the Western Indian Ocean (Roxy et al. 2014), which indicates that ENSO dominates the western tropical Indian Ocean variability through atmospheric

Fig. 3 SST anomaly ($^{\circ}\text{C}$, color contour) and Steering flows (black arrows) for Nisarga during (a) pre-cyclonic, (b) cyclonic, and (c) post-cyclonic period and for Nanauk during (d) pre-cyclonic, (e) cyclonic, and (f) post-cyclonic period



teleconnections. Rhein et al. (2014) showed that 90% of the heat resulting from global warming during the last four decades has accumulated in the oceans. The periodic occurrence of El Niño events out of this heat causes a partial transfer of heat to the Indian Ocean via a modified Walker circulation and is reflected in the warming trend over the region. The tropical Indian Ocean basin-wide warming occurred in 2020, following an extremely positive IOD event, however, 2014 was a negative IOD year (Figure not shown). A weak to moderate El Niño event occurs in 2014–2015, whereas 2020–2021 was a moderate La Niña year (figure not shown). Both these IOD and ENSO controlled the variation of ocean temperature in the Arabian Sea during the cyclone formation stage. The combined effect of these factors could be the possible reason for stronger SST anomaly in the west Arabian Sea during the pre-condition of the Nanauk cyclone. SST anomaly during the cyclonic period showed (Fig. 3b, e) reduced SST and also negative SST anomaly near both the storm center. Because of ocean mixing by wind-driven upwelling (Jacob et al. 2000; Price 2009), SST typically drops during the passage of TC. This SST further decreases (Fig. 3c for

Nisarga; Fig. 3f for Nanauk) with the propagation of the storm in the post-cyclonic period. Lower SST limits the supply of ocean heat flux into TC, which hinders further intensification of the storm (Black et al. 2007; Lin et al. 2008). Bongirwar et al. (2011) showed that instead of SST, horizontal SST gradient acts as the more crucial driving force for the intensification and movement of tropical cyclones over the Indian Ocean. Figure S2 shows the SST gradient for the pre, during, and post-cyclonic periods over the Arabian Sea for both cyclonic storms, which further supports our results of SST. Moreover, the SST anomaly (Fig. S3) and actual SST (Fig. S4) have been plotted for six consecutive days for Nisarga (May 31 to June 4, 2020) and Nanauk (9–14 June 2014), respectively. It is clearly seen in Fig. S2 that the SST gradient was more uniform for the case of Nisarga compared to Nanauk, which may be due to positive IOD during the year 2020. As both the storm continue to intensify, the SST decreased drastically for Nanauk which suppressed the storm from further intensification, whereas for Nisarga, the SST magnitude was high enough to fuel more energy to the storm.

In addition, environmental steering flow (black arrows in Fig. 3), which helps in the movement of tropical cyclones, can be described as the synoptic-scale flow surrounding the cyclone. The pressure level at which the speed and direction of the surrounding winds best correlate with those of the cyclone is called the steering level. George and Gray (1976) suggested that TC track is a function of deep-layer wind field. They averaged winds between 1 and 7° radius and found that the winds at 500 hPa and 700 hPa have the strongest correlation with the direction of cyclone movement and speed of cyclone, respectively. Though different studies describe the environmental steering flow differently (Dong and Neumann 1986; George and Gray 1976; Velden and Leslie 1991), mostly it is considered as the wind averaged through two or more atmospheric levels. Optimum steering flow can be obtained by varying the vertical depth of the steering layer and radius which can successfully explain the track of the storm (Galarneau and Davis 2013). In this study, wind is averaged from 850 to 300 hPa level, to calculate environmental steering flow. In Fig. 3, anti-clockwise environmental steering (black arrows) shows the wind flow pattern for the mid-tropospheric mean layer for both the storms at pre-cyclonic, cyclonic, and post-cyclonic periods. Less prominent circulation patterns were visible during the pre-cyclonic period for Nisarga (Fig. 3a) and for Nanauk (Fig. 3d). This anti-clockwise wind pattern further becomes more prominent during the cyclonic period (3b for Nisarga and 3e for Nanauk) at the storm center near the north-eastern Arabian Sea. The anti-clockwise circulation faded away in the post-cyclonic period for both Nisarga (Fig. 3c) and Nanauk (Fig. 3f). No significant difference in the environmental steering flow strength is found for the two cyclonic storms in this study. As the wind speed and direction is often determined by the interaction of large-scale features, the motion, and structure of tropical cyclone are not only controlled by steering flow but also by nearby synoptic features (Carr and Elsberry 2000; Wu et al. 2004). In addition, latent heat release associated with cyclonic convection can play an important role in cyclonic motion by modifying the ambient environment (Anwender et al. 2008; Harr et al. 2008; Henderson et al. 1999). Divergent outflow from the convection can also distort the potential vorticity via advection (Archambault et al. 2013), which further leads to change in the upper tropospheric wind and hence the steering flow (Bassill 2014; Torn et al. 2015).

4.2 Latent heat flux

Various theoretical, observational, and model-based studies showed that LHF at the air–sea interface acts as the primary energy source and provides the fuel to TC genesis and development (Bao et al. 2000; Emanuel 1986; Gao et al. 2017; Jaimes et al. 2015; Ooyama 1969; Wu et al. 2005;

Zhang et al. 2018). Negative LHF in Fig. 4 near the north-eastern Arabian Sea for Nisarga (a–f) and Nanauk (g–l), signifies strong evaporation from the ocean surface towards the atmosphere during the time of storm intensification. This negative LHF fueled both storms to intensify further. Wind-induced surface heat exchange (WISHE) mechanism (Emanuel 1986; 1989; 1997) pointed out the important role of sea surface heat fluxes during TC intensification. Montgomery et al. (2009, 2015) examined the WISHE mechanism by artificially suppressing the feedback between the surface heat fluxes and the surface wind speed. This study revealed that a storm with suppressed heat fluxes would eventually reach a weaker steady-state intensity. Thus, as the upward LHF for the storm Nanauk (Fig. 4g–l) started decreasing from 12 June 2014 onwards, it hinders further moisture supply and resulted in the storm dissipation. The surface wind speed and the heat fluxes simultaneously increase during the rapid intensification phase (Miyamoto and Takemi 2013), suggesting that the WISHE mechanism plays a crucial role in the rapid intensification of the storm. For the case of Nisarga (Fig. 4a–f), starting from 1 to 3 June 2020 the upward negative flux continuously sourced energy to the storm, which helped the storm to further intensify. As the TC moved towards the land in the post-cyclonic period, the LHF magnitude decreased over the ocean but increased over land following the TC track.

4.3 Specific humidity

Theoretical as well as modeling studies established that an ample amount of atmospheric moisture (Emanuel et al. 2004; Kimball 2006), especially high mid-tropospheric humidity acts as a crucial factor for the genesis, intensification, and development of maximum intensity of cyclonic storms (Gray 1979; Hendricks et al. 2010; Li et al. 2012; Shu et al. 2012; Wu et al. 2012). However, the intrusion of dry air can lower or suppress TC intensification (Emanuel 1989). Specific humidity anomaly averaged over 850 hPa to 550 hPa is analyzed in this study to understand the role of moisture in tropical cyclonic storms. In the case of Nisarga, it is clear that (Fig. 5a–c) environmental moisture content increased from the pre-cyclonic period to the cyclonic period, which intensified the cyclone, and helped the storm to further propagate. After the passage of the cyclone, atmospheric moisture decreased over the eastern Arabian Sea. Humidity increased from pre-cyclonic to cyclonic stages in the case of Nanauk (Fig. 5d–f) also. Positive specific humidity anomaly averaged from 850 to 550 hPa showed that the atmospheric moisture supply from low to mid-level was ample for Nanauk similar to Nisarga, which helps to supply the moisture content to the storm. As we know, surface latent heat flux is directly proportional to specific humidity (Cronin et al. 2019) which can be denoted by Eq. 1:

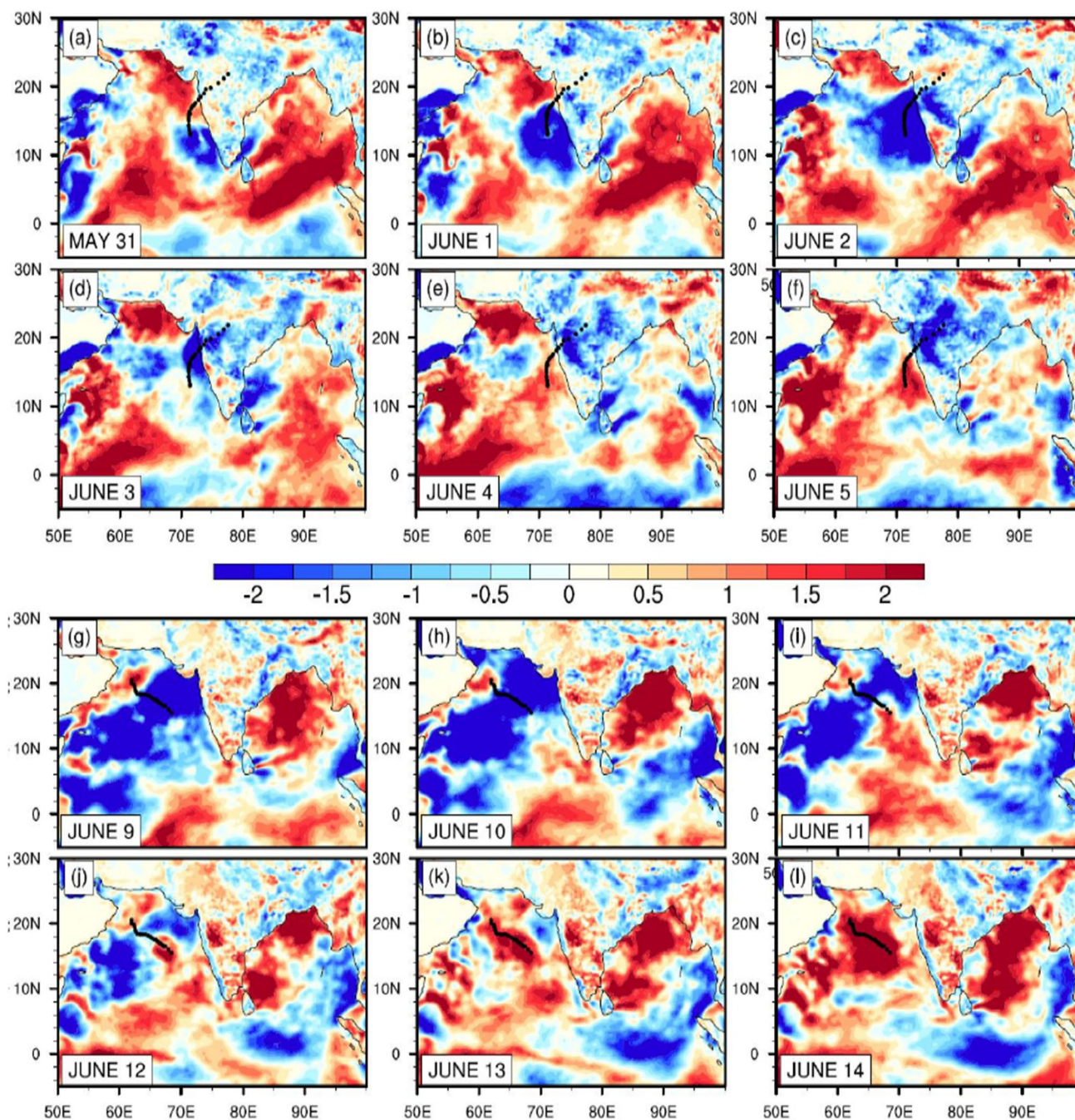


Fig. 4 Latent heat flux ($J m^{-2}$): from 31 May to 5 June 2020 for cyclone Nisarga (a–f) and from 9 to 14 June 2014 for cyclone Nanauk (g–l)

$$Q_{lat} = \rho L_v \langle wq \rangle \tag{1}$$

where Q_{lat} denotes latent heat flux, ρ is the air density, L_v is the latent heat of evaporation, w is vertical velocity, q is specific humidity, and the brackets denote the temporal average. The results in this study also affirm the direct relationship between LHF and specific humidity variation for both cyclonic storms. As the LHF increases (more negative

anomaly), evaporation increases from the ocean surface to the atmosphere which supply the moisture to the storms through increasing atmospheric humidity.

4.4 Relative vorticity

Vorticity is the tendency for elements of the fluid to spin, which can be denoted by Eq. 2:

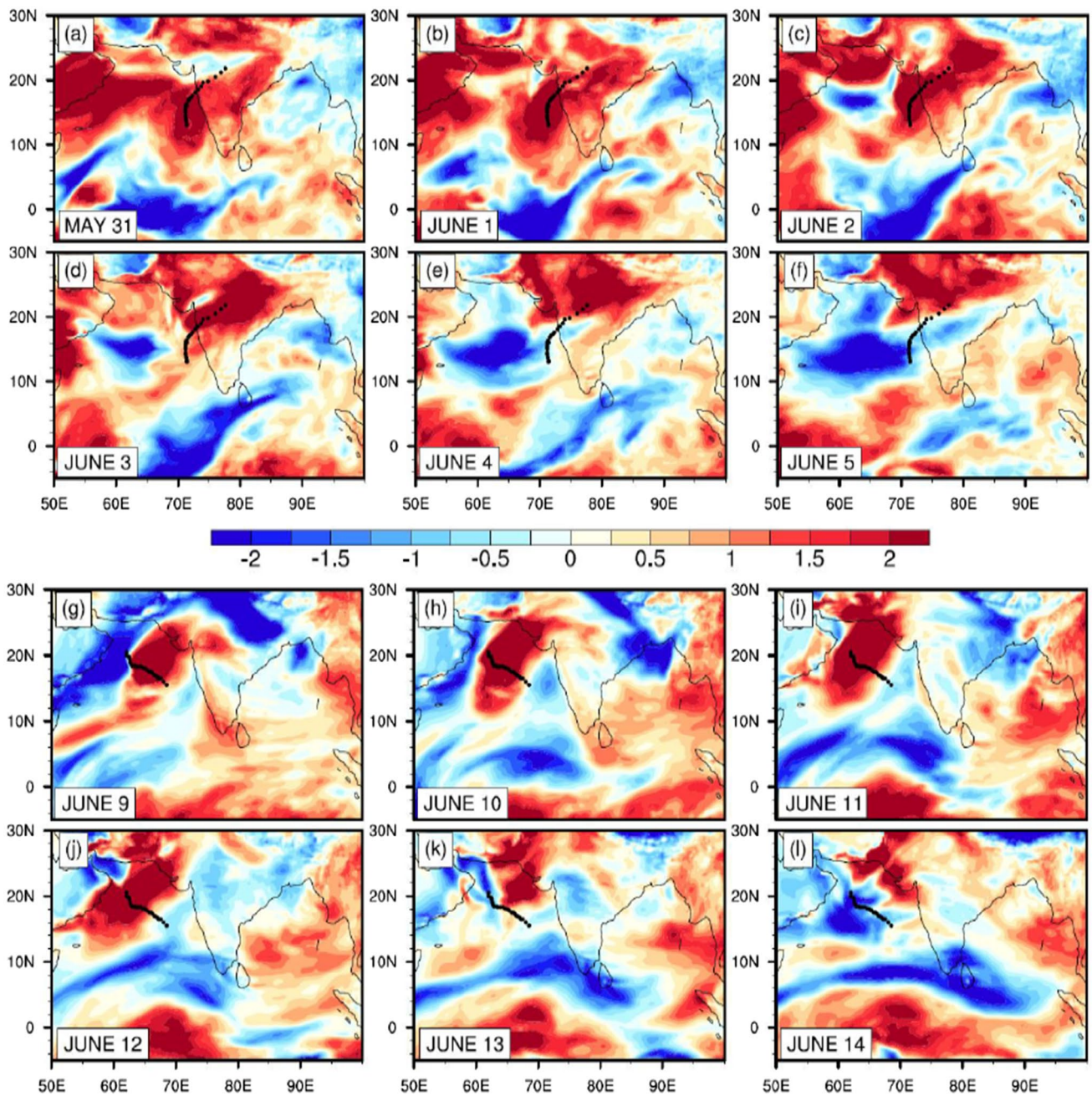


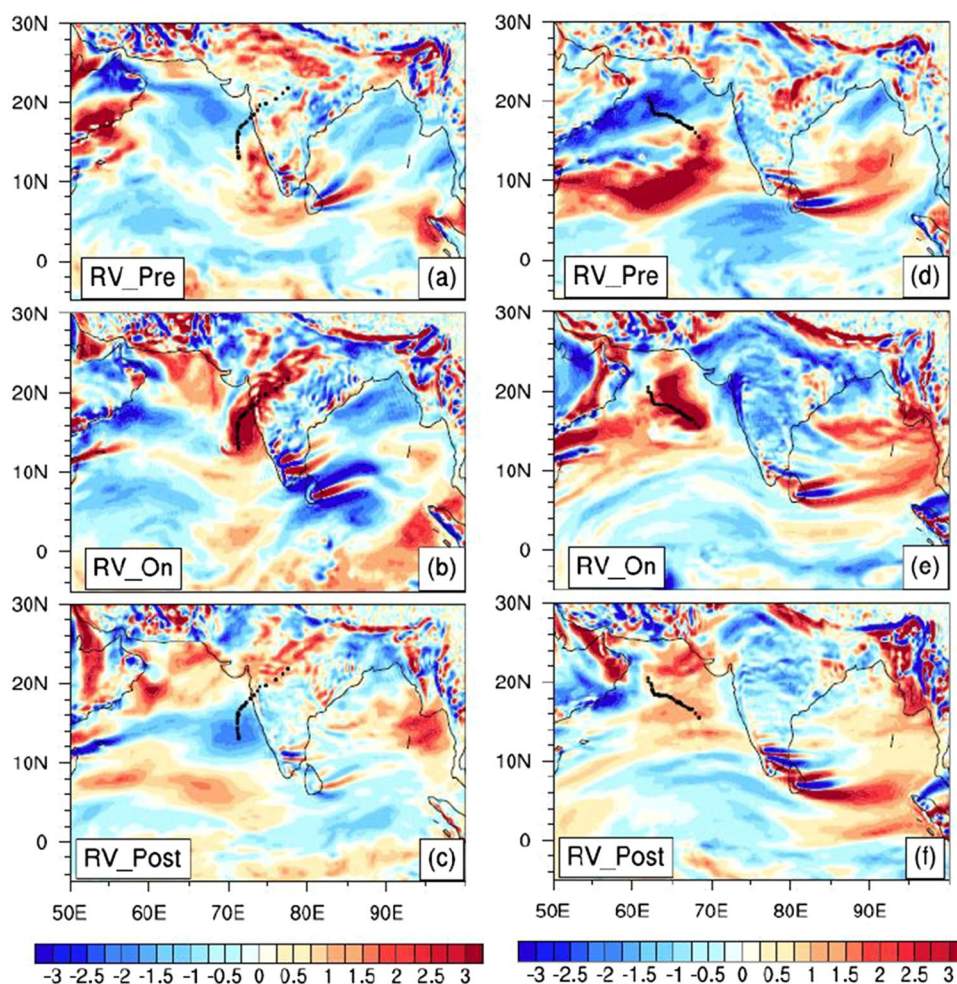
Fig. 5 Specific humidity (kg kg^{-1} , averaged over 850 hPa to 550 hPa): from 31 May to 5 June 2020 for cyclone Nisarga (a–f) and from 9 to 14 June 2014 for cyclone Nanauk (g–l)

$$\begin{aligned} \frac{D}{Dt}(\zeta + f) = & -(\zeta + f)\left(\frac{\partial u}{\partial x} + \frac{\partial v}{\partial y}\right) - \left(\frac{\partial w}{\partial x} \frac{\partial v}{\partial z} - \frac{\partial w}{\partial y} \frac{\partial u}{\partial z}\right) \\ & + \frac{1}{\rho^2} \left(\frac{\partial \rho}{\partial x} \frac{\partial p}{\partial y} - \frac{\partial \rho}{\partial y} \frac{\partial p}{\partial x}\right) \end{aligned} \tag{2}$$

where ζ denotes relative vorticity, f is the Coriolis parameter, p is pressure, ρ is the atmospheric density, u , v , and w are the components of wind velocity. In the vorticity equation

(Eq. 2), the first term on the right-hand side (RHS) denotes advection, the second term contributes to tilting and the third term is the solenoid term. Hence, it is clear from the equation (Eq. 2) that relative vorticity (RV) not only plays a crucial role in the spinning of tropical cyclones but can also control the path or the track of cyclones through the tilting term. In this study, relative vorticity (10^{-5} s^{-1}) anomaly at 850 hPa for Nisarga in pre-cyclonic (Fig. 6a), cyclonic (Fig. 6b), and post-cyclonic (Fig. 6c) periods showed large

Fig. 6 Relative vorticity (s^{-1} , 850 hPa) anomaly: Nisarga during (a) pre-cyclonic, (b) cyclonic, and (c) post-cyclonic stage and Nanauk during (d) pre-cyclonic, (e) cyclonic, and (f) post-cyclonic stage



low-level positive anomaly during the cyclonic period which gradually increased from the pre-cyclonic period and finally decreased as a negative anomaly during the post-cyclonic stage. For the cyclonic storm Nisarga, a similar situation resulted in increased low-level cyclonic vorticity, which further led to the propagation and intensification of the storm eastward. Weak positive relative vorticity anomaly resulted in a controlled movement and track of the tropical cyclone Nanauk (Fig. 6d–f).

4.5 Vertical wind shear

Figure 7a–f shows low vertical wind shear (VWS) through the Nisarga cyclonic track with the minimum at the storm center. Low vertical wind shear along with other atmospheric and oceanic parameters helped the storm Nisarga to develop gradually from deep depression to severe cyclone. However, before the intensification of Nanauk, the VWS anomaly was low (Fig. 7g–i). VWS anomaly increased gradually from pre-cyclonic stages to cyclonic stages, which became positive from 11 June 2014 onwards. Large vertical wind shear is responsible for the hindrance of the genesis

of TC and also weakens the storm (Paterson et al. 2005; Wang et al. 2015; Zeng et al. 2007, 2008, 2010), hence, it has to be within the threshold value for a TC intensification (Gallina and Velden 2002; Ritchie 2002; Zehr 1992). VWS ventilates the inner portion of the storm, which advects away heat and moisture from the storm center and inhibits the storm development (Gray 1968). These prevailing conditions caused faster dissipation of cyclone Nanauk.

4.6 Convective available potential energy

In the case of the Nisarga cyclone (Fig. 8a–f), from 29 to 31 May 2020 during the intensification stage, the magnitude of CAPE showed a high value ($> 1000 \text{ J kg}^{-1}$) over the region of the eastern Arabian Sea. It is a known fact that before the intensification of the cyclone, CAPE increases (Lee and Frisius 2018; Montgomery and Smith 2014; Schecter 2011; Sang et al. 2008), which acts as the source of energy for convection, which further affects the release of latent heat and strengthens the developing storm. For the Nisarga cyclone, CAPE was conducive for the intensification of the storm with high SST anomalies, large specific humidity, increased

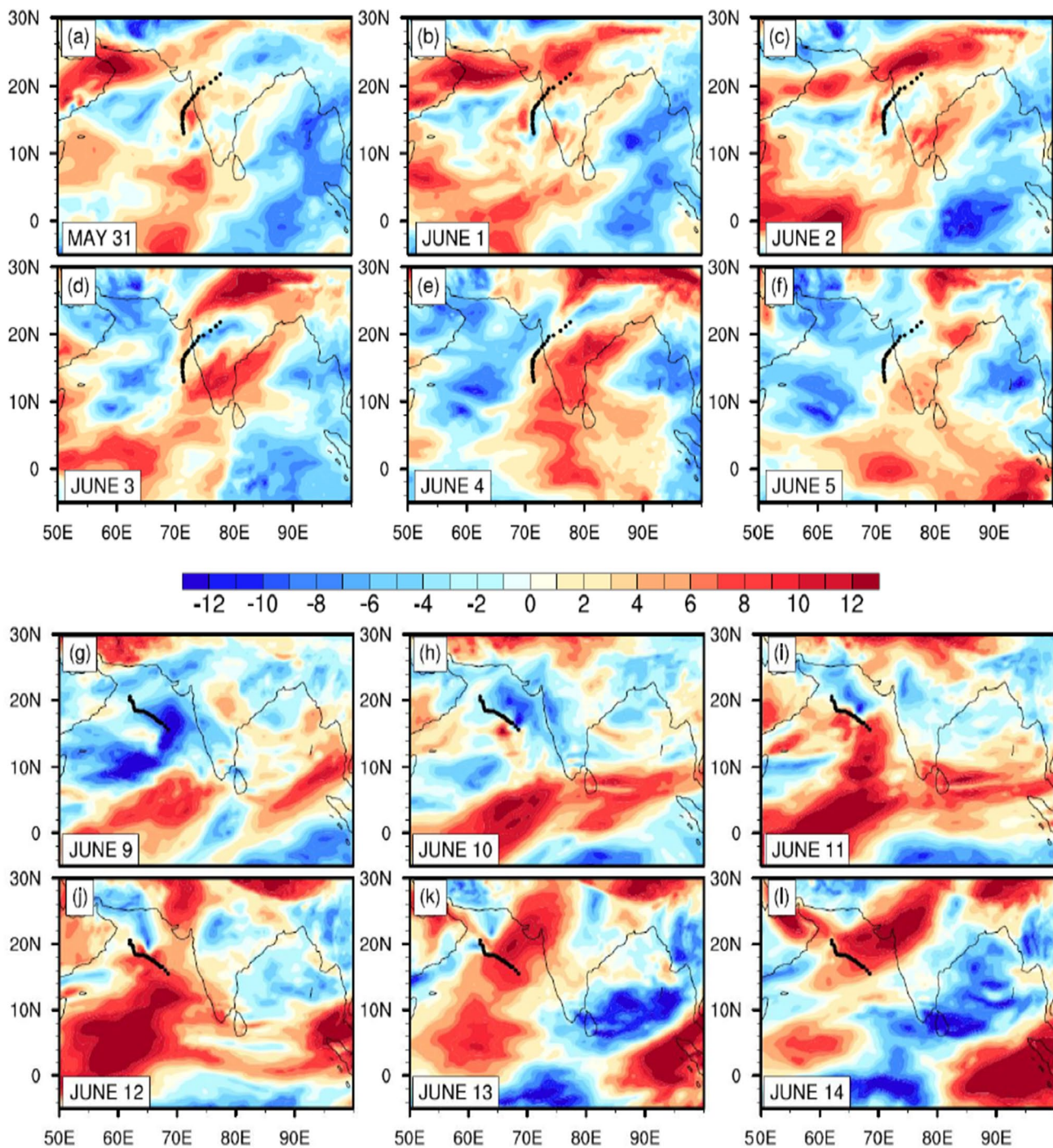


Fig. 7 Vertical wind shear (ms^{-1}) of zonal wind between 250 and 850 hPa for Nisarga from 31 May to 5 June 2020 (a–f) and for Nanauk from 9 to 14 June 2014 (g–l)

relative vorticity, and large latent heating flux. A combination of these factors along with increased CAPE over the region, helped the atmosphere to be more thermodynamically unstable. These thermodynamic conditions over the eastern Arabian Sea helped the system to undergo rapid intensification. Studies also showed that (Lee and Frisius

2018) both the initial amount of CAPE as well as the CAPE that is generated at the time of storm intensification have an impact on the storm. This was not prominent in the case of Nanauk (Fig. 8g–l), where the weak anomaly of CAPE did not provide enough strength for the storm to further intensify.

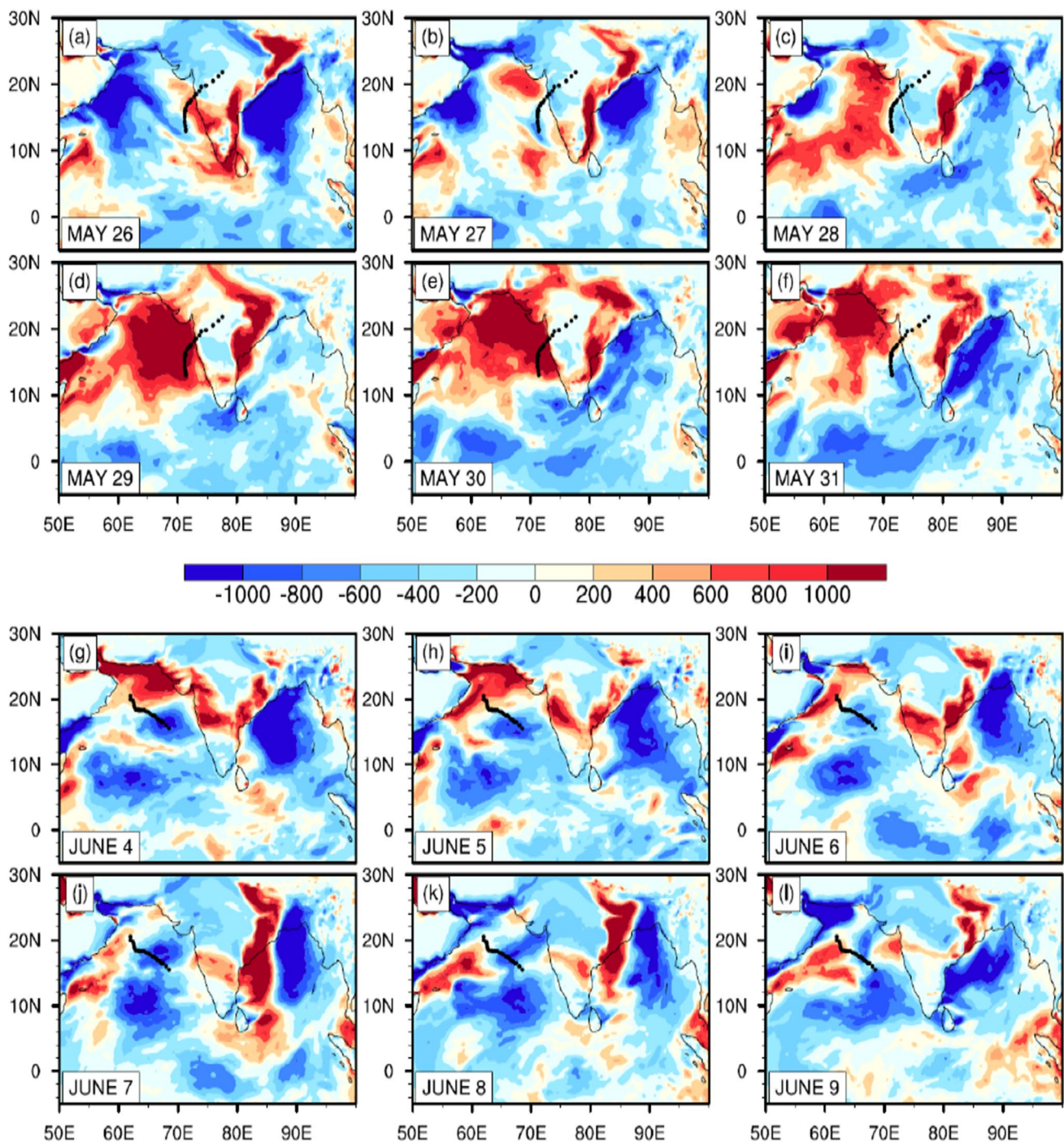


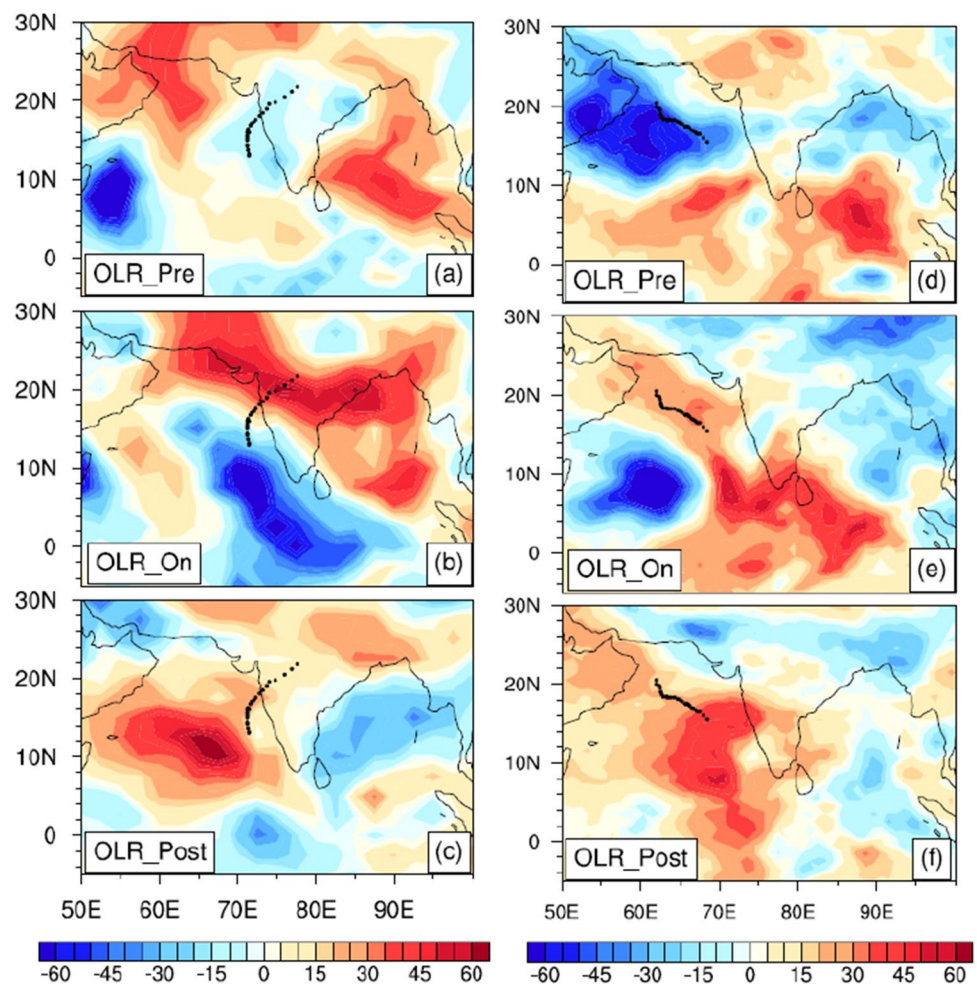
Fig. 8 CAPE (J kg^{-1}) from 26 to 31 May 2020 for cyclone Nisarga (a–f) and from 4 to 9 June 2014 for cyclone Nanauk (g–l)

4.7 Outgoing longwave radiation

Often OLR acts as a proxy for convection. A convectively active (suppressed) region with a higher cloud emits less amount of radiation into space which is indicated by a negative (positive) value of OLR. OLR anomaly for CS Nisarga in pre-cyclonic, cyclonic, and post-cyclonic periods (Fig. 9)

is analyzed in this study. A clear difference is observed between pre-cyclonic (Fig. 9a) and post-cyclonic (Fig. 9c) storms with negative and positive OLR values, respectively, over the eastern Arabian Sea, whereas during the active storm period (Fig. 9b), the strong convective activity is depicted by a much higher negative OLR value. More convective activity in the eastern Arabian Sea implies higher

Fig. 9 OLR anomaly (W/m^2) for Nisarga during (a) pre-cyclonic, (b) cyclonic, and (c) post-cyclonic stage and for Nanauk during (d) pre-cyclonic, (e) cyclonic, and (f) post-cyclonic stage



cloud tops. Higher cloud tops are colder which emits less radiation into space. Negative OLR anomaly helps in convection and the storm to intensify into CS, but for Nanauk, as the storm progressed from the pre-cyclonic to the cyclonic and post-cyclonic period (Fig. 9d–f), with time the OLR showed positive anomaly throughout the cyclonic track. Hence, though in the pre-cyclonic period, negative OLR depicted increased convection, which helped the storm to intensify into a cyclonic storm, negative anomaly afterward weakened the convection which resulted in the dissipation of the storm drastically.

4.8 Role of MJO

MJO is an eastward-moving band of convection in the tropics. MJO plays an important role in the genesis and propagation of cyclones (Krishnamohan et al. 2012). MJO provides favorable atmospheric conditions to TCs (Klotzbach 2014). In the convective phase of MJO, the equatorial lower tropospheric westerly wind gets stronger at the west side of the convection which provides a favorable environment for tropical cyclones propagation by increasing

cyclonic vorticity (Rui and Wang 1990). Regions through the MJO passes typically show enhanced convective activity. In Fig. 10a, the MJO phase diagram is plotted starting from 10 May to 15 June 2020. The green line shows the MJO index for the month of May, and the red is for the month of June. The axes denote 1 to 8 different phases along with the magnitude (-4 to 4) of MJO. A magnitude more than 1 is considered as MJO associated with stronger convection. As we can see from Fig. 10a, starting from 30 May the MJO is propagating from the African landmass towards the Western Indian Ocean. This MJO condition provides a background for enhanced convective activity in the western Arabian Sea and a favorable environment for intensifying storm activity. In addition, the strong lower tropospheric westerly wind which is associated with the MJO at the west side of the storm, helped it in eastward propagation. Thus, MJO played an important role in the intensification and growth of the storm Nisarga. In Fig. 10b, the propagation of MJO from 1 to 20 June 2014 is shown by the green line for the cyclonic storm Nanauk. Starting from 1 June, the MJO was propagating through the central Indian Ocean to the east Indian Ocean, with a

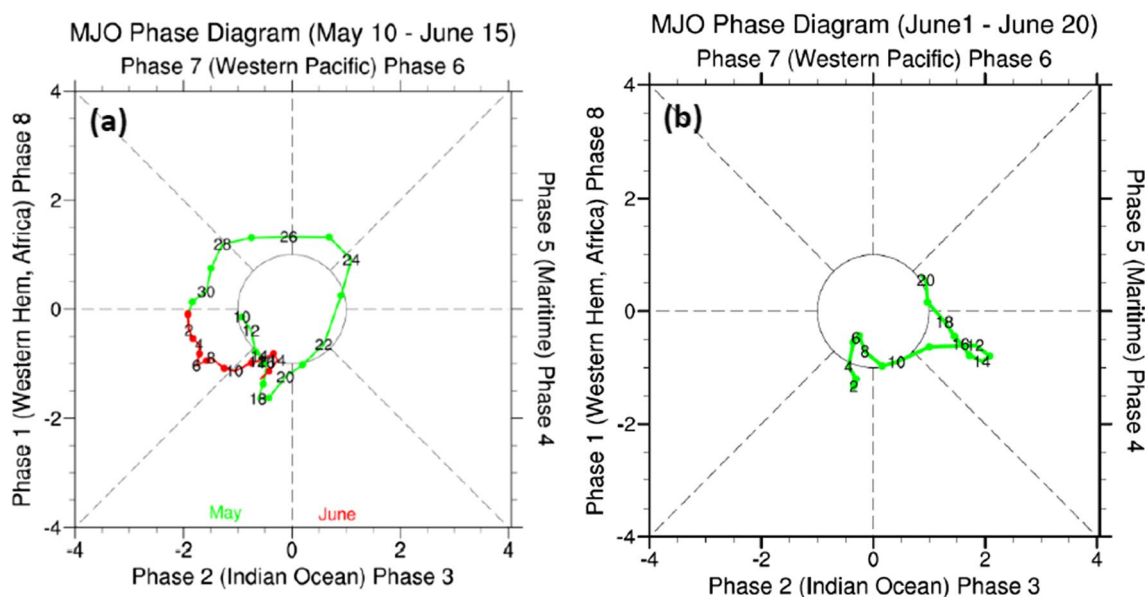


Fig. 10 MJO phase diagram from 10 May (green) to 15 June (red), 2020 for Nisarga (a) and from 1 to 20 June 2014 for Nanauk (b)

very low magnitude. This MJO environment was unable to contribute to the intensification of cyclone Nanauk. Hence, the position, as well as the magnitude of MJO convection, played a crucial role in the diverse characteristics of these two comparable cyclonic storms.

5 Discussion and conclusion

Momentum and moisture transfer between the ocean surface and atmosphere is the major driving force for tropical cyclones while passing through the ocean. This study aimed to analyze the role of air–sea interaction on the genesis, development, and propagation of two tropical cyclones to understand the underlying causes resulting in different characteristics of them. Nisarga, the first ever tropical severe cyclone over the Arabian Sea since 1891 in the month of June hit the Maharashtra coast, and Nanauk, a cyclonic storm moved northwestward in the Arabian Sea. Even though both originated from an almost similar location in the Arabian Sea, their characteristics were entirely different. Not only the intensity, but their track of movement also differed from each other. The change in surface wind speed in Nisarga showed that it gradually increased for a period of ~30 h and then slowly decreased, whereas for Nanauk, the change in surface wind speed showed that it increased only for ~12 h then suddenly decreased and became static for almost 24 h before decaying. Though the SST anomaly was high before the intensification for both the CSs, the LHF which helps in exchanging energy from ocean to atmosphere decreased drastically for Nanauk which resulted in making

the cyclone static and suddenly decay. However, in the case of Nisarga, the pre-cyclonic LHF anomaly, which was slightly positive, increased drastically during the cyclonic period. This fueled Nisarga cyclonic storm to intensify into a severe cyclonic storm and helped in its further development. Moreover, favorable MJO conditions provided conducive background winds that helped to improve the growth of Nisarga. Analysis of various atmospheric and oceanic parameters in the pre-cyclonic, cyclonic, and post-cyclonic periods also indicated favorable conditions for the genesis and intensification of Nisarga over the eastern Arabian Sea. Anomalously warm SST anomaly of about 1.2–1.4 °C around the genesis center and high CAPE ($> 1000 \text{ J kg}^{-1}$) in the pre-cyclonic period fueled the Nisarga storm, enhancing convective activity over the region. In addition, the low vertical wind shear provided a favorable environment for the genesis of the storm. Further, cyclonic storm Nisarga intensified rapidly to a severe cyclonic storm on 3rd June 2020 due to favorable thermodynamic conditions in the southeast Arabian Sea. An increase in relative vorticity at low-level, mid-tropospheric humidity, and latent heat flux during the cyclonic period along with low vertical wind shear helped the storm to prevail and intensify into a severe cyclonic storm. A high-pressure anticyclonic circulation over the east of the system in the Indian landmass dragged the cyclonic storm north-eastward across the Maharashtra coast. The convective phase of MJO along with the strong lower tropospheric westerly wind at the west of the convective system additionally helped the cyclone to propagate eastward. This convective phase of MJO is associated with negative OLR anomaly resulting in increased total surface

precipitation over the region. CAPE which can enhance the potential to form active convection was not very high before the intensification of Nanauk. Negative OLR anomaly typically helps in convection and the storm to intensify into CS, but with time the OLR showed positive anomaly throughout the cyclonic track of Nanauk. In summary, low LHF, active southwest monsoon surge, positive wind shear anomaly, and low value of CAPE played a crucial role in dampening the cyclonic storm Nanauk. MJO was in phase 3 for Nanauk, with very low strength, which could not support the storm Nanauk to further intensify. An in-depth analysis of the present study highlighted that ocean–atmosphere interactions played a crucial role in the genesis, intensification, and propagation of cyclonic storms. Lack of understanding and weak ocean–atmosphere coupling can cause uncertainties in the cyclone forecasting models. Hence, this study highlights the importance of the representation of ocean–atmosphere coupling in cyclone forecasting models for better prediction skills.

Supplementary Information The online version contains supplementary material available at <https://doi.org/10.1007/s00703-023-00987-w>.

Acknowledgements The authors are grateful to the reviewers for their valuable suggestions. The authors acknowledge the India Meteorological Department (IMD) Regional Specialised Meteorological Centre (RSMC), Optimum Interpolation Sea Surface Temperature (OISST), and Australian Bureau of Meteorology for providing the required data for this study. European Centre for Medium-Range Weather Forecasts (ECMWF) is acknowledged for providing ECMWF Re-Analysis (ERA-interim) data. The authors are grateful for the support of the head, of CSIR 4PI. The first author of the paper is supported by a grant from CSIR-NCP (Grant No.31-2(281)/2021-22/Bud).

Data availability All the datasets used in this study are obtained from open source as acknowledged.

References

- Anwender D, Harr PA, Jones SC (2008) Predictability associated with the downstream impacts of the extratropical transition of tropical cyclones: case studies. *Mon Weather Rev* 136:3226–3247. <https://doi.org/10.1175/2008MWR2249.1>
- Archambault HM, Bosart LF, Keyser D, Cordeira JM (2013) A climatological analysis of the extratropical flow response to recurving western north pacific tropical cyclones. *Mon Weather Rev* 141:2325–2346. <https://doi.org/10.1175/MWR-D-12-00257.1>
- Bao JW, Wilczak JM, Choi JK, Kantha LH (2000) Numerical simulations of air-sea interaction under high wind conditions using a coupled model: a study of hurricane development. *Mon Weather Rev* 128:2190–2210. [https://doi.org/10.1175/1520-0493\(2000\)128%3C2190:NSOASI%3E2.0.CO;2](https://doi.org/10.1175/1520-0493(2000)128%3C2190:NSOASI%3E2.0.CO;2)
- Bassill NP (2014) Accuracy of early GFS and ECMWF sandy (2012) track forecasts: evidence for a dependence on cumulus parameterization. *Geophys Res Lett* 41:3274–3281. <https://doi.org/10.1002/2014GL059839>
- Beal LM, Vialard J, Roxy MK et al (2020) A road map to IndoOS-2: better observations of the rapidly warming Indian Ocean. *Bull Am Meteorol Soc* 101:E1891–E1913. <https://doi.org/10.1175/BAMS-D-19-0209.1>
- Black PG, D'asaro EA, Drennan WM et al (2007) Air-sea exchange in hurricanes: synthesis of observations from the coupled boundary layer air-sea transfer experiment. *Bull Am Meteorol Soc* 88:357–374. <https://doi.org/10.1175/BAMS-88-3-357>
- Bongirwar V, Rakesh V, Kishtawal CM et al (2011) Impact of satellite observed microwave SST on the simulation of tropical cyclones. *Nat Hazards* 58:929–944. <https://doi.org/10.1007/s11069-010-9699-y>
- Braun SA, Sippel JA, Shie CL, Boller RA (2013) The Evolution and role of the saharan air layer during Hurricane Helene (2006). *Mon Weather Rev* 141:4269–4295. <https://doi.org/10.1175/MWR-D-13-00045.1>
- Burpee RW, Black ML (1989) Temporal and spatial variations of rainfall near the centers of two tropical cyclones. *Mon Weather Rev* 117:2204–2218. [https://doi.org/10.1175/1520-0493\(1989\)117%3c2204:TASVOR%3e2.0.CO;2](https://doi.org/10.1175/1520-0493(1989)117%3c2204:TASVOR%3e2.0.CO;2)
- Carr LE, Elsberry RL (2000) Dynamical tropical cyclone track forecast errors. Part I: tropical region error sources. *Weather Forecast* 15:641–661. [https://doi.org/10.1175/1520-0434\(2000\)015%3c0641:DTCTFE%3e2.0.CO;2](https://doi.org/10.1175/1520-0434(2000)015%3c0641:DTCTFE%3e2.0.CO;2)
- Charney JG, Eliassen A (1964) On the growth of the hurricane depression. *J Atmos Sci* 21:68–75. [https://doi.org/10.1175/1520-0469\(1964\)021%3c0068:OTGOTH%3e2.0.CO;2](https://doi.org/10.1175/1520-0469(1964)021%3c0068:OTGOTH%3e2.0.CO;2)
- Chen X, Wang Y, Zhao K (2015) Synoptic flow patterns and large-scale characteristics associated with rapidly intensifying tropical cyclones in the South China Sea. *Mon Weather Rev* 143:64–87. <https://doi.org/10.1175/mwr-d-13-00338.1>
- Chowdary JS, Gnanaseelan C (2007) Basin-wide warming of the Indian Ocean during El Niño and Indian Ocean dipole years. *Int J Climatol* 27(11):1421–1438. <https://doi.org/10.1002/joc.1482>
- Chowdhury RR, Kumar SP, Narvekar J, Chakraborty A (2020) Back-to-back occurrence of tropical cyclones in the Arabian Sea during October–November 2015: causes and responses. *J Geophys Res Oceans* 125:1–23. <https://doi.org/10.1029/2019JC015836>
- Collins M et al (2019) Extremes, abrupt changes and managing risks. In IPCC Special Report on Oceans and Cryosphere in a Changing Climate (eds Portner et al., 2019).
- Cronin MF, Gentemann CL, Edson J et al (2019) Air-sea fluxes with a focus on heat and momentum. *Front Mar Sci* 6:434858. <https://doi.org/10.3389/fmars.2019.00430>
- Dee DP, Uppala SM, Simmons AJ et al (2011) The ERA-Interim reanalysis: configuration and performance of the data assimilation system. *Q J R Meteorol Soc* 137:553–597. <https://doi.org/10.1002/qj.828>
- DeMaria M (1996) The effect of vertical shear on tropical cyclone intensity change. *J Atmos Sci* 53:2076–2088. [https://doi.org/10.1175/1520-0469\(1996\)053%3c2076:TEOVSO%3e2.0.CO;2](https://doi.org/10.1175/1520-0469(1996)053%3c2076:TEOVSO%3e2.0.CO;2)
- DeMaria M, Sampson CR, Knaff JA, Musgrave KD (2014) Is tropical cyclone intensity guidance improving? *Bull Am Meteorol Soc* 95:387–398. <https://doi.org/10.1175/BAMS-D-12-00240.1>
- Deo AA, Ganer DW, Nair G (2011) Tropical cyclone activity in global warming scenario. *Nat Hazards* 59:771–786. <https://doi.org/10.1007/s11069-011-9794-8>
- Dong K, Neumann CJ (1986) The relationship between tropical cyclone motion and environmental geostrophic flows. *Mon Weather Rev* 114:115–122. [https://doi.org/10.1175/1520-0493\(1986\)114%3c0115:TRBTCM%3e2.0.CO;2](https://doi.org/10.1175/1520-0493(1986)114%3c0115:TRBTCM%3e2.0.CO;2)
- Dube SK, Jain I, Rao AD, Murty TS (2009) Storm surge modelling for the Bay of Bengal and Arabian Sea. *Nat Hazards* 51:3–27. <https://doi.org/10.1007/s11069-009-9397-9>
- Emanuel KA (1986) An air-sea interaction theory for tropical cyclones. Part I: steady state maintenance. *J Atmos Sci*

- 43:585–605. <https://doi.org/10.1175/1520-0469%281986%29043%3C0585%3AAASITF%3E2.0.CO%3B2>
- Emanuel KA (1989) The finite-amplitude nature of tropical cyclogenesis. *J Atmos Sci* 46:3431–3456. [https://doi.org/10.1175/1520-0469\(1989\)046%3c3431:TFANOT%3e2.0.CO;2](https://doi.org/10.1175/1520-0469(1989)046%3c3431:TFANOT%3e2.0.CO;2)
- Emanuel KA (1997) Some aspects of hurricane inner-core dynamics and energetics. *J Atmos Sci* 54:1014–1026. [https://doi.org/10.1175/1520-0469\(1997\)054%3C1014:SAOHIC%3E2.0.CO;2](https://doi.org/10.1175/1520-0469(1997)054%3C1014:SAOHIC%3E2.0.CO;2)
- Emanuel KA (1999) Thermodynamic control of hurricane intensity. *Nature* 401:665–669. <https://doi.org/10.1038/44326>
- Emanuel KA (2000) A statistical analysis of tropical cyclone intensity. *Mon Weather Rev* 128:1139–1152. [https://doi.org/10.1175/1520-0493\(2000\)128%3c1139:ASAOTC%3e2.0.CO;2](https://doi.org/10.1175/1520-0493(2000)128%3c1139:ASAOTC%3e2.0.CO;2)
- Emanuel K (2005) Increasing destructiveness of tropical cyclones over the past 30 years. *Nature* 436:686–688. <https://doi.org/10.1038/nature03906>
- Emanuel K (2007) Environmental factors affecting tropical cyclone power dissipation. *J Clim* 20:5497–5509. <https://doi.org/10.1175/2007JCLI1571.1>
- Emanuel KA (2017) Will global warming make hurricane forecasting more difficult? *Bull Am Meteorol Soc* 98:495–501. <https://doi.org/10.1175/BAMS-D-16-0134.1>
- Emanuel K, DesAutels C, Holloway C, Korty R (2004) Environmental control of tropical cyclone intensity. *J Atmos Sci* 61:843–858. [https://doi.org/10.1175/1520-0469\(2004\)061%3C0843:ECOTCI%3E2.0.CO;2](https://doi.org/10.1175/1520-0469(2004)061%3C0843:ECOTCI%3E2.0.CO;2)
- Enagonio J, Montgomery MT (2001) Tropical cyclogenesis via convectively forced vortex rossby waves in a shallow water primitive equation model. *J Atmos Sci* 58:685–706. [https://doi.org/10.1175/1520-0469\(2001\)058%3c0685:TCVCFV%3e2.0.CO;2](https://doi.org/10.1175/1520-0469(2001)058%3c0685:TCVCFV%3e2.0.CO;2)
- Galarneau TJ Jr, Davis CA (2013) Diagnosing forecast errors in tropical cyclone motion. *Mon Weather Rev* 141:405–430. <https://doi.org/10.1175/MWR-D-12-00071.1>
- Gallina GM, Velden CS (2002) Environmental vertical wind shear and tropical cyclone intensity change utilizing enhanced satellite derived wind information. Extended Abstracts, 25th Conf. on Hurricanes and Tropical Meteorology, San Diego, CA, Amer Meteor Soc, 172–173.
- Gao S, Zhai S, Chen B, Li T (2017) Water budget and intensity change of tropical cyclones over the western North Pacific. *Mon Weather Rev* 145:3009–3023. <https://doi.org/10.1175/MWR-D-17-0033.1>
- George JE, Gray WM (1976) Tropical cyclone motion and surrounding parameter relationships. *J Appl Meteorol Climatol* 15:1252–1264. [https://doi.org/10.1175/1520-0450\(1976\)015%3c1252:TCMASP%3e2.0.CO;2](https://doi.org/10.1175/1520-0450(1976)015%3c1252:TCMASP%3e2.0.CO;2)
- Gray WM (1968) Global view of the origin of tropical disturbances and storms. *Mon Weather Rev* 96:669–700. [https://doi.org/10.1175/1520-0493\(1968\)096%3c0669:GVOTOO%3e2.0.CO;2](https://doi.org/10.1175/1520-0493(1968)096%3c0669:GVOTOO%3e2.0.CO;2)
- Gray WM (1979) Hurricanes: their formation, structure and likely role in the tropical circulation. In: Shaw DB (ed) *Meteorology Over the Tropical Oceans*. Royal Meteorological Society, London, pp 155–218
- Groisman P, Knight R, Karl T, Easterling D, Sun B, Lawrimore J (2004) Contemporary changes of the hydrological cycle over the contiguous United States: trends derived from in situ observations. *J Hydrometeorol* 5:64–85. [https://doi.org/10.1175/1525-7541\(2004\)005%3c0064:CCOTH%3e2.0.CO;2](https://doi.org/10.1175/1525-7541(2004)005%3c0064:CCOTH%3e2.0.CO;2)
- Harr PA, Anwender D, Jones SC (2008) Predictability associated with the downstream impacts of the extratropical transition of tropical cyclones: Methodology and a case study of Typhoon Nabi (2005). *Mon Weather Rev* 136:3205–3225. <https://doi.org/10.1175/2008MWR2248.1>
- Henderson JM, Lackmann GM, Gyakum JR (1999) An analysis of Hurricane Opal's forecast track errors using quasi geostrophic potential vorticity inversion. *Mon Weather Rev* 127:292–307. [https://doi.org/10.1175/1520-0493\(1999\)127%3c0292:AAO-HOS%3e2.0.CO;2](https://doi.org/10.1175/1520-0493(1999)127%3c0292:AAO-HOS%3e2.0.CO;2)
- Hendricks EA, Peng MS, Fu B, Li T (2010) Quantifying environmental control on tropical cyclone intensity change. *Mon Weather Rev* 138:3243–3271. <https://doi.org/10.1175/2010MWR3185.1>
- India Meteorological Department. Cyclone atlas—tracks of cyclones and depressions over north Indian Ocean (from 1891 onwards) 2011. Electronic version 2.0/2011 Cyclone Warnings and Research Center, India Meteorological Department, Chennai.
- Izumo T, Montegut CB, Luo JJ, Behera SK, Masson S, Yamagata T (2008) The role of the western Arabian Sea upwelling in Indian monsoon rainfall variability. *J Clim* 21:5603–5623. <https://doi.org/10.1175/2008JCLI2158.1>
- Jacob SD, Shay LK, Mariano AJ, Black PG (2000) The 3D oceanic mixed layer response to Hurricane Gilbert. *J Phys Oceanogr* 30:1407–1429. [https://doi.org/10.1175/1520-0485\(2000\)030%3c1407:TOMLRT%3e2.0.CO;2](https://doi.org/10.1175/1520-0485(2000)030%3c1407:TOMLRT%3e2.0.CO;2)
- Jaimes B, Shay LK, Uhlhorn EW (2015) Enthalpy and momentum fluxes during Hurricane Earl relative to underlying ocean features. *Mon Weather Rev* 143:111–131. <https://doi.org/10.1175/MWR-D-13-00277.1>
- Kimball SK (2006) A modeling study of hurricane landfall in a dry environment. *Mon Weather Rev* 134:1901–1918. <https://doi.org/10.1175/MWR3155.1>
- Klotzbach PJ (2006) Trends in global tropical cyclone activity over the past twenty years (1986–2005). *Geophys Res Lett* 33:1984–1987. <https://doi.org/10.1029/2006GL025881>
- Klotzbach PJ (2014) The Madden–Julian Oscillation's impacts on worldwide tropical cyclone activity. *J Clim* 27:2317–2330. <https://doi.org/10.1175/JCLI-D-13-00483.1>
- Knapp KR, Kruk MC, Levinson DH, Diamond HJ, Neumann CJ (2010) The international best track archive for climate stewardship (IBTrACS) unifying tropical cyclone data. *Bull Am Meteorol Soc* 91:363–376. <https://doi.org/10.1175/2009BAMS2755.1>
- Komaromi WA (2013) An investigation of composite Dropsonde profiles for developing and nondeveloping tropical waves during the 2010 PREDICT field campaign. *J Atmos Sci* 70:542–558. <https://doi.org/10.1175/JAS-D-12-052.1>
- Kossin JP, Knapp KR, Olander TL, Velden CS (2020) Global increase in major tropical cyclone exceedance probability over the past four decades. *Proc Natl Acad Sci USA* 117:11975–11980. <https://doi.org/10.1073/pnas.1920849117>
- Krishnamohan KS, Mohanakumar K, Joseph PV (2012) The influence of Madden–Julian Oscillation in the genesis of north Indian Ocean tropical cyclones. *Theor Appl Climatol* 109:271–282. <https://doi.org/10.1007/s00704-011-0582-x>
- Lee M, Frisius T (2018) On the role of convective available potential energy (CAPE) in tropical cyclone intensification. *Tellus a: Dyn Meteorol Oceanogr* 70:1433433. <https://doi.org/10.1080/1600870.2018.1433433>
- Li K, Yu W, Li T, Murty VSN, Khokiattiwong S, Adi TR, Budi S (2012) Structures and mechanisms of the first-branch northward-propagating intraseasonal oscillation over the tropical Indian Ocean. *Clim Dyn* 40:1707–1720. <https://doi.org/10.1007/s00382-012-1492-z>
- Li Z, Yu W, Li T et al (2013) Bimodal character of cyclone climatology in the Bay of Bengal modulated by monsoon seasonal cycle. *J Clim* 26:1033–1046. <https://doi.org/10.1175/JCLI-D-11-00627.1>
- Lin I, Wu C, Pun I, Ko D (2008) Upper-ocean thermal structure and the western North Pacific category 5 typhoons. Part I: Ocean features and the Category 5 Typhoons' intensification. *Mon Weather Rev* 136:3288–3306. <https://doi.org/10.1175/2008MWR2277.1>
- Madden RA, Julian PR (1971) Detection of a 40–50 day oscillation in the zonal wind in the tropical Pacific. *J Atmos Sci* 28:702–708.
- Maloney ED, Hartmann DL (2001) The Madden–Julian oscillation, barotropic dynamics, and North Pacific tropical cyclone

- formation. Part I: Observations *J Atmos Sci* 58:2545–2558. [https://doi.org/10.1175/1520-0469\(2001\)058%3c2545:TMJOB%3e2.0.CO;2](https://doi.org/10.1175/1520-0469(2001)058%3c2545:TMJOB%3e2.0.CO;2)
- McBride JL (1995) Tropical cyclone formations. Chapter 3 of *Global Perspectives on Tropical Cyclones*. Being published by WMO, 57 pp.
- Miyamoto Y, Takemi T (2013) A transition mechanism for the spontaneous axisymmetric intensification of tropical cyclones. *J Atmos Sci* 70:112–129. <https://doi.org/10.1175/JAS-D-11-0285.1>
- Mohanty S, Nadimpalli R, Osuri KK, Pattanayak S, Mohanty U, Sil S (2019) Role of sea surface temperature in modulating life cycle of tropical cyclones over Bay of Bengal. *Trop Cyclone Res Rev* 8:68–83. <https://doi.org/10.1016/j.tcr.2019.07.007>
- Mohapatra M, Bandyopadhyay BK, Nayak DP (2013a) Evaluation of operational tropical cyclone intensity forecasts over north Indian Ocean issued by India Meteorological Department. *Nat Hazards* 68:433–451. <https://doi.org/10.1007/s11069-013-0624-z>
- Mohapatra M, Nayak DP, Sharma RP, Bandyopadhyay BK (2013b) Evaluation of official tropical cyclone track forecast over north Indian Ocean issued by India Meteorological Department. *J Earth Syst Sci* 122:589–601. <https://doi.org/10.1007/s12040-013-0291-1>
- Mohapatra M, Nayak DP, Sharma M, Sharma RP, Bandyopadhyay BK (2015) Evaluation of official tropical cyclone landfall forecast issued by India Meteorological Department. *J Earth Syst Sci* 124:861–874. <https://doi.org/10.1007/s12040-015-0581-x>
- Mohapatra GN, Rakesh V, Mohanty PK, Himesh S (2018) Comparative evaluation of the skill of a global circulation model and a limited area model in simulating tropical cyclones in the North Indian Ocean. *Meteorol Appl* 25:523–533. <https://doi.org/10.1002/met.1718>
- Mohapatra M, Geetha B, Sharma M (2017) Reduction in uncertainty in tropical cyclone track forecasts over the North Indian Ocean. *Curr Sci* 112:1826–1830. <https://doi.org/10.18520/cs/v112/i09/1826-1830>
- Montgomery MT, Sang NV, Smith RK, Persing J (2009) Do tropical cyclones intensify by WISHE? *Q J R Meteorol Soc* 135:1697–1714. <https://doi.org/10.1002/qj.459>
- Montgomery MT, Persing J, Smith RK (2015) Putting to rest WISHEful misconceptions for tropical cyclone intensification. *J Adv Model Earth Syst* 7:92–109. <https://doi.org/10.1002/2014M000362>
- Montgomery MT, Smith RK (2014) Paradigms for tropical cyclone intensification. *Aust Meteorol Oceanogr J* 64:37–66. <https://doi.org/10.22499/2.6401.005>
- Murakami H, Vecchi GA, Underwood S (2017) Increasing frequency of extremely severe cyclonic storms over the Arabian Sea. *Nat Clim Change* 7:885–889. <https://doi.org/10.1038/s41558-017-0008-6>
- Needham HF, Keim BD, Sathiaraj D (2015) A review of tropical cyclone-generated storm surges: global data sources, observations, and impacts. *Rev Geophys* 53:545–591. <https://doi.org/10.1002/2014RG000477>
- Neumann CJ (1992) The joint Typhoon Warning Center (JTWC92) model. SAIC, Final Report, 85 pp.
- Ooyama KV (1969) Numerical simulation of the life cycle of tropical cyclones. *J Atmos Sci* 26:3–40. [https://doi.org/10.1175/1520-0469\(1969\)026%3c0003:nsotlc%3e2.0.co;2](https://doi.org/10.1175/1520-0469(1969)026%3c0003:nsotlc%3e2.0.co;2)
- Paterson LA, Hanstrum BN, Davidson NE, Weber HC (2005) Influence of environmental vertical wind shear on the intensity of hurricane-strength tropical cyclones in the Australian region. *Mon Weather Rev* 133:3644–3660. <https://doi.org/10.1175/mwr3041.1>
- Price JF (2009) Metrics of hurricane-ocean interaction: vertically-integrated or vertically-averaged ocean temperature? *Ocean Sci* 5:351–368. <https://doi.org/10.5194/os-5-351-2009>
- Rappaport EN (2000) Loss of life in the United States associated with recent atlantic tropical cyclones. *Bull Am Meteorol Soc* 81:2065–2074. [https://doi.org/10.1175/1520-0477\(2000\)081%3c2065:LOLITU%3e2.3.CO;2](https://doi.org/10.1175/1520-0477(2000)081%3c2065:LOLITU%3e2.3.CO;2)
- Reynolds RW, Smith TM, Liu C, Chelton DB, Casey KS, Schlax MG (2007) Daily high-resolution-blended analyses for sea surface temperature. *J Clim* 20:5473–5496. <https://doi.org/10.1175/2007jcli1824.1>
- Rhein M, and Coauthors (2014) *Observations: Ocean*. *Climate Change 2013: The Physical Science Basis*, T. F. Stocker et al., Eds., Cambridge University Press, 255–315.
- Ritchie EA (2002). Topic 1.2: Environmental effects. Topic Chairman and Rapporteur Reports of the Fifth WMO International Workshop on Tropical Cyclones IWTC-V, WMO Tech. Doc. WMO/ TD 1136.
- Rogers R, Chen SS, Tenerelli J, Willoughby H (2003) A numerical study of the impact of vertical shear on the distribution of rainfall in Hurricane Bonnie (1998). *Mon Weather Rev* 131:1577–1599. <https://doi.org/10.1175//2546.1>
- Roxy MK, Ritika K, Terray P, Masson S (2014) The curious case of indian ocean warming. *J Clim* 27:8501–8509. <https://doi.org/10.1175/JCLI-D-14-00471.1>
- Roxy MK, Ritika K, Terray P, Murtugudde R, Ashok K, Goswami BN (2015) Drying of Indian subcontinent by rapid Indian ocean warming and a weakening land-sea thermal gradient. *Nat Commun* 6:1–10. <https://doi.org/10.1038/ncomms8423>
- Roxy MK, Dasgupta P, McPhaden MJ, Suematsu T, Zhang C, Kim D (2019) Twofold expansion of the Indo-Pacific warm pool warps the MJO lifecycle. *Nature* 575:647–651. <https://doi.org/10.1038/s41586-019-1764-4>
- Rui H, Wang B (1990) Development characteristics and dynamic structure of tropical intraseasonal convection anomalies. *J Atmos Sci* 47:357–379. [https://doi.org/10.1175/1520-0469\(1990\)047%3c0357:dcadso%3e2.0.co;2](https://doi.org/10.1175/1520-0469(1990)047%3c0357:dcadso%3e2.0.co;2)
- Sanap SD, Mohapatra M, Ali MM, Priya P, Varaprasad D (2020) On the dynamics of cyclogenesis, rapid intensification and recurvature of the very severe cyclonic storm. Ockhi *J Earth Syst Sci* 129:194. <https://doi.org/10.1007/s12040-020-01457-2>
- Sang NV, Smith RK, Montgomery MT (2008) Tropical cyclone intensification and predictability in three dimensions. *Q J R Meteorol Soc* 134:563–582. <https://doi.org/10.1002/qj.235>
- Schecter DA (2011) Evaluation of a reduced model for investigating hurricane formation from turbulence. *Q J R Meteorol Soc* 137:155–178. <https://doi.org/10.1002/qj.729>
- Sebastian M, Behera MR (2015) Impact of SST on tropical cyclones in North Indian Ocean. *Procedia Eng* 116:1072–1077. <https://doi.org/10.1016/j.proeng.2015.08.346>
- Shephard JM, Grundstein A, Mote TL (2007) Quantifying the contribution of tropical cyclones to extreme rainfall along the coastal southeastern United States. *Geophys Res Lett* 34:810. <https://doi.org/10.1029/2007GL031694>
- Shu S, Ming J, Chi P (2012) Large-scale characteristics and probability of rapidly intensifying tropical cyclones in the western North Pacific basin. *Weather Forecast* 27:411–423. <https://doi.org/10.1175/waf-d-11-00042.1>
- Singh VK, Roxy MK (2020a) A review of the ocean-atmosphere interactions during tropical cyclones in the north Indian Ocean. *ArXiv*. <https://arxiv.org/abs/2012.04384>
- Singh VK, Roxy MK, Deshpande M (2020b) The unusual long track and rapid intensification of very severe cyclone Ockhi. *Curr Sci* 119:771–779. <https://doi.org/10.18520/cs/v119/i5/771-779>
- Sobel AH, Camargo SJ, Hall TM, Lee CY, Tippettk MK, Wing AA (2016) Human influence on tropical cyclone intensity. *Science* 353:242–246. <https://doi.org/10.1126/science.aaf6574>

- Torn RD, Whitaker JS, Pegion P, Hamill TM, Hakim GJ (2015) Diagnosis of the source of GFS medium-range track errors in Hurricane Sandy (2012). *Mon Weather Rev* 143:132–152. <https://doi.org/10.1175/MWR-D-14-00086.1>
- Velden CS, Leslie LM (1991) The basic relationship between tropical cyclone intensity and the depth of the environmental steering layer in the Australian region. *Weather Forecast* 6:244–253. [https://doi.org/10.1175/1520-0434\(1991\)006%3c0244:TBRBTC%3e2.0.CO;2](https://doi.org/10.1175/1520-0434(1991)006%3c0244:TBRBTC%3e2.0.CO;2)
- Wang Y, Wu CC (2004) Current understanding of tropical cyclone structure and intensity changes—a review. *Meteorol Atmospheric Phys* 87:257–278. <https://doi.org/10.1007/s00703-003-0055-6>
- Wang Y, Rao Y, Tan ZM, Schonemann D (2015) A statistical analysis of the effects of vertical wind shear on tropical cyclone intensity change over the western North Pacific. *Mon Weather Rev* 143:3434–3453. <https://doi.org/10.1175/mwr-d-15-0049.1>
- Webster P (2008) Myanmar's deadly daffodil. *Nat Geosci* 1:488–490. <https://doi.org/10.1038/ngeo257>
- Wheeler MC, Hendon HH (2004) An all-season real-time multivariate MJO index: development of an index for monitoring and prediction. *Mon Weather Rev* 132:1917–1932. [https://doi.org/10.1175/1520-0493\(2004\)132%3C1917:AARMMI%3E2.0.CO;2](https://doi.org/10.1175/1520-0493(2004)132%3C1917:AARMMI%3E2.0.CO;2)
- Wing AA, Sobel AH, Camargo SJ (2007) Relationship between the potential and actual intensities of tropical cyclones on interannual time scales. *Geophys Res Lett* 34:L08810. <https://doi.org/10.1029/2006gl028581>
- Wu CC, Huang TS, Chou KH (2004) Potential vorticity diagnosis of the key factors affection the motion of Typhoon Sinlaku (2002). *Mon Weather Rev* 132:2084–2093. [https://doi.org/10.1175/1520-0493\(2004\)132%3C2084:PVDOTK%3E2.0.CO;2](https://doi.org/10.1175/1520-0493(2004)132%3C2084:PVDOTK%3E2.0.CO;2)
- Wu L, Wang B, Braun SA (2005) Impacts of air-sea interaction on tropical cyclone track and intensity. *Mon Weather Rev* 133:3299–3314. <https://doi.org/10.1175/mwr3030.1>
- Wu L, Su H, Fovell RG et al (2012) Relationship of environmental relative humidity with North Atlantic tropical cyclone intensity and intensification rate. *Geophys Res Lett* 39:L20809. <https://doi.org/10.1029/2012GL053546>
- Xing W, Huang F (2013) Influence of summer monsoon on asymmetric bimodal pattern of tropical cyclogenesis frequency over the Bay of Bengal. *J Ocean Univ China* 12:279–286. <https://doi.org/10.1007/s11802-013-2219-4>
- Yanase W, Satoh M, Taniguchi H, Fujinami H (2012) Seasonal and intraseasonal modulation of tropical cyclogenesis environment over the Bay of Bengal during the extended summer monsoon. *J Clim* 25:2914–2930. <https://doi.org/10.1175/JCLI-D-11-00208.1>
- Zawislak JA (2013) Necessary and sufficient conditions for tropical cyclogenesis, PhD dissertation. 215 pp., The Univ. of Utah, Salt Lake City. Zehr, R.M., 1992. Tropical cyclogenesis in the western North Pacific, NOAA Tech. Rep. NESDIS 61, 181 pp., U. S. Dep. of Commer. Washington, D. C.
- Zehr RM (1992) Tropical Cyclogenesis in the Western North Pacific. NOAA Technical Report NESDIS6, National Oceanic and Atmospheric Administration, Washington DC, 181 p.
- Zeng Z, Wang Y, Wu CC (2007) Environmental dynamical control of tropical cyclone intensity—an observational study. *Mon Weather Rev* 135:38–59. <https://doi.org/10.1175/mwr3278.1>
- Zeng Z, Chen LS, Wang Y (2008) An observational study of environmental dynamical control of tropical cyclone intensity in the North Atlantic. *Mon Weather Rev* 136:3307–3322. <https://doi.org/10.1175/2008mwr2388.1>
- Zeng Z, Wang Y, Chen LS (2010) A statistical analysis of vertical shear effect on tropical cyclone intensity change in the North Atlantic. *Geophys Res Lett* 37:L02802. <https://doi.org/10.1029/2009gl041788>
- Zhang J, Liu P, Zhang F, Song Q (2018) CloudNet: Ground-based cloud classification with deep convolutional neural network. *Geophys Res Lett* 45:8665–8672. <https://doi.org/10.1029/2018gl077787>

Publisher's Note Springer Nature remains neutral with regard to jurisdictional claims in published maps and institutional affiliations.

Springer Nature or its licensor (e.g. a society or other partner) holds exclusive rights to this article under a publishing agreement with the author(s) or other rightsholder(s); author self-archiving of the accepted manuscript version of this article is solely governed by the terms of such publishing agreement and applicable law.